DOI: 10.1002/ ((please add manuscript number))
Article type: Full Paper

Tuning the Luminescence of Tin Oxide Low Dimensional Structures in the Near Infrared Range by in-situ doping during a Vapor-Solid Growth Process

*Miguel García-Tecedor[1], Félix del Prado[1], Dorcas Torres[2], David Maestre[1] and Ana Cremades[1]**

Dedicated to Professor Javier Piqueras

[1]Departamento Física de Materiales, Facultad de Físicas, Universidad Complutense de Madrid, Madrid 28040, Spain
[2]Natural Science and Mathematics Department, Inter American University, Bayamon, Puerto Rico

*E-mail: cremades@fis.ucm.es

Keywords: vapor-solid, tin oxide, cathodoluminescence

Abstract

Tin oxide low dimensional structures increasingly attract attention due to their wide application area. Indeed, by attaining new morphologies and properties the potential applications might increase the device portfolio. Furthermore, an adequate combination of doped SnO_2 nano- and microstructures could enable multi-functionality and totally new applications. The latter might be the case of low dimensional tin oxide structures emitting in the near infrared range, which is below the energy of the common visible luminescence of tin oxide. The ability to obtain near infrared luminescence from tin oxide is tested by doping in-situ during a vapor-solid growth using Li, Cu and Cr containing precursors in the initial mixture with tin oxide or metallic tin powders. Luminescence around 1.5 eV is obtained for all the samples with morphologies varying from microtubes to rods and belts depending on the specific dopant and the Sn-based precursor.

1. Introduction

Tin oxide is a wide band gap material with E_g around 3,6 eV which presents applications in gas sensors,[1] solar cells,[2] catalysis,[3] batteries[4] or as a diluted magnetic semiconductor (DMSO),[5] among others. Many of these applications can be improved by reducing the size of tin oxide and by adequate doping. The controlled doping of nanostructures is a difficult task in which great efforts are invested, as it is of high relevance for the control of the performance of SnO_2-based devices. Tin nanostructures such as nanoparticles, belts, plates

and wires have been successfully doped with different elements such as the transition metal chromium,[6-7] vanadium,[8-9] and manganese.[10-11] Other elements such as rare earths are also commonly used to dope tin oxide, being erbium a paradigmatic example.[12-13] Less attention has been paid so far to other doping elements such as copper.[14] The interest in doping tin oxide with copper is usually based on its behaviour as an oxidative catalyst for hydrocarbons to achieve a considerable degree of sensitivity and selectivity, improving the response to H_2S in gas sensors.[15] Moreover, co-doping with different elements can lead to overcome limitations of single-doped SnO_2 and widen the applicability of SnO_2.[16-17]

Recently, other low dimensional structures of transparent conducting oxides (TCO) such as micro and nanotubes are attracting increasing attention due to their improved performances in energy storage, among others.[18] Its fabrication by template-based methods,[19] gives rise to polycrystalline and mesoporous, instead of highly crystalline materials. On the contrary, the TCO tubes grown by an analogous vapor-solid method used in this work,[20-24] are single crystalline and do not need the use of a catalyst. Doping with different elements efficiently influences the optical properties of TCO tubular structures, which can be used for different applications, for example, as a luminescence material for the visible range or as optical resonator combined with wave-guiding behaviour.[23, 25]

In this work, we have achieved the doping of SnO_2 elongated nano and microstructures with Cu, as well as the codoping with Li and Cr by a vapor-solid method. The influence of the Sn-based precursor material and the doping in the size, shape and morphology of the as-grown structures is demonstrated, as well as the ability to shift the luminescence of tin oxide into the near infrared region, for which the best results are obtained for Li and Cr codoped tubular microstructures. The luminescence emission of tin oxide is commonly reported as a wide emission in the visible range[26] comprising several complex bands related to intrinsic defects, mainly oxygen vacancies. Therefore, the ability to tune the luminescence of tin oxide tubes in

the NIR could be useful in sensors and biochemical detection,[27] widening the applicability of tin oxide.

2. Results and discussion

Undoped tin oxide low dimensional structures have been achieved starting from SnO_2 powders at 1400ºC, by a vapor solid growth as reported elsewhere.[21] The preferential morphologies obtained by this method are microtubes, with lateral (110) surfaces and <001> growth directions, as determined by electron backscatter diffraction (EBSD) and Raman polarized measurements.[28-29] The growth mechanism is based on the anisotropy of the rutile tin oxide structure for which the most stable surface is the {110}.[23] These microtubes can be doped during growth with Li or Cr by incorporating the convenient element in the powder precursors, while maintaining the tube morphology with slight changes.[28-29] In the case of codoping with Li and Cr, the surface of the pellet is fully covered by microstructures after the thermal treatments performed at 1400 ºC during 10h, as it can be observed in Figure 1a. The majority of these structures are microtubes, although there is a small amount of other morphologies such as microrods and microplates. The amount of microtubes in the Cr-Li codoped samples is higher than in the undoped SnO_2 ones. In Figure 1(b-c) some of these tubular microstructures can be observed with higher magnification. The microtubes show square or rectangular cross-sections with widths between 50 and 200 μm and lengths up to 5 mm. The co-doping process with Cr and Li in SnO_2 introduces some morphological changes in the structures as compared to undoped material. First of all, the length of the as-grown microstructures was increased with the Cr-Li codoping, as compared with undoped or separately Li or Cr doped tubes.

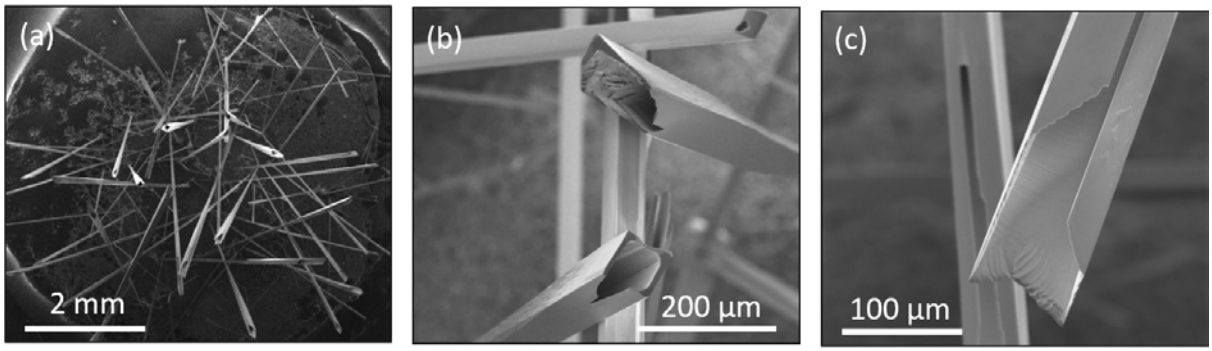

Figure 1. (a) SEM image of the aspect of the SnO_2:Cr,Li pellet after the thermal treatment. (b), (c) and (d) SEM images showing different codoped SnO_2:Cr,Li microtubes.

The co-doped samples seem to have simultaneously the morphological influence of both Cr and Li dopants. To get a better understanding of this fact, in Figure 2, a comparison of undoped and differently doped SnO_2 microtubes is shown.

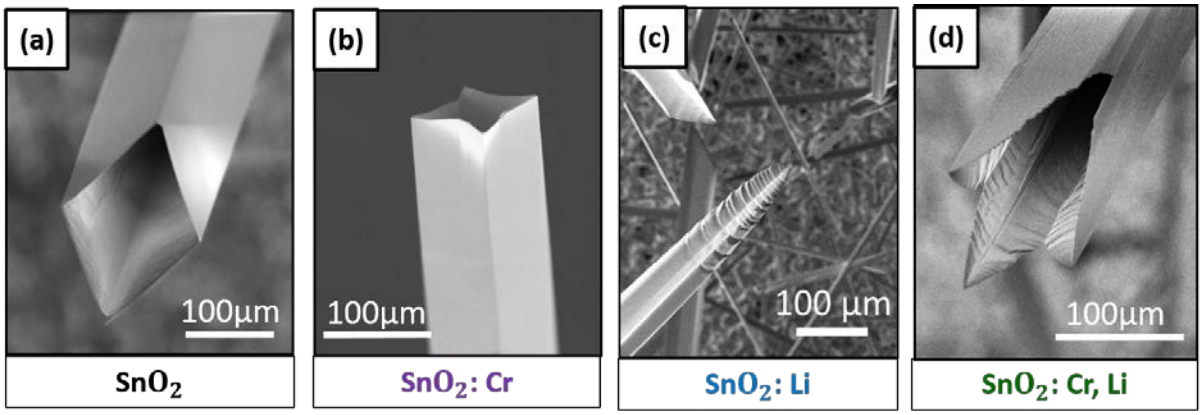

Figure 2. SEM images of (a) undoped, (b) Cr doped, (c) Li doped and (d) Cr and Li co-doped SnO_2 microtubes.

As it can be observed in Figure 2, different SEM images show the evolution of the morphological aspect of the as-grown microtubes by the introduction of different dopants. In Figure 2(a) an undoped SnO_2 microtube can be observed with square cross-section, no angular ending and smooth inner and outer surfaces. In Figure 2(b), a Cr doped structure is shown where a characteristic angular four tip-ending can be observed. These four tip-ending microtubes were also observed in Cr doped rutile TiO_2 microtubes.[20] In Figure 2(c) Li doped

SnO_2 microstructures are observed, where a *snake tail*-ending can be observed as it was previously reported.[28] Finally, in Figure 2(d), the aspect of a Cr and Li co-doped microtube is shown, where a mixture of the four-tip (three in that case because the fourth tip is missing in this structure) and the snake tail ending can be observed.

In order to study the crystalline structure of the as-grown microtubes some of them were carefully detached from the pellet surface and analyzed by XRD. Figure 3(a) shows the XRD measurements acquired in both undoped and Li and Cr codoped microtubes for comparison. XRD measurements confirm that the codoped SnO_2:Cr,Li microtubes consist of cassiterite SnO_2 with tetragonal rutile structure, as the undoped ones. No presence of any ternary compounds or any rest of precursor powders has been detected by this technique. The preferential crystalline orientations belong to the family planes {110}, in agreement with the results for undoped, Cr doped and Li doped SnO_2 microtubes.[28-29] Therefore, the doping process does not vary the growth direction and the family of planes, which form the lateral surfaces of the microtubes.

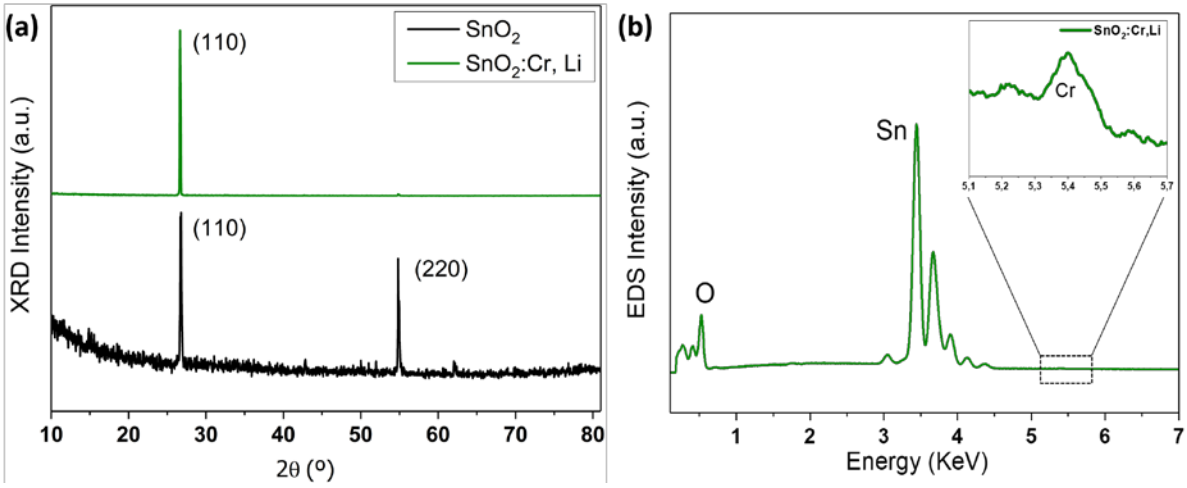

Figure 3. XRD patterns acquired on undoped and codoped SnO_2:Cr,Li samples and (b) EDS spectrum from the codoped SnO_2:Cr,Li sample.

The chemical composition of the microtubes was also analyzed in terms of EDS measurements. The EDS spectrum acquired in the codoped SnO_2:Cr,Li sample is shown in Figure 3(b). Peaks corresponding to Sn and O can be clearly observed. The inset in Figure 4 shows an enlarged region of the spectrum where a weak peak corresponding to Cr K_α lines can be observed, confirming the presence of Cr in the analyzed microtubes. The amount of Cr incorporated in these microstructures is below 1% at, as estimated from the quantification of the corresponding EDS spectrum. Moreover, Cr is homogeneously distributed along the microtubes according to EDS measurements and in agreement with previous works.[7, 29] On the other hand, as lithium is a light element it cannot be detected by the EDS technique. However, due to the observed morphology modifications similarly to the reference SnO_2:Li samples, the Li incorporation in the codoped microstructures is assumed to be achieved as previously demonstrated by different techniques[28] for the reference SnO_2:Li tubes. The achievement of simultaneous incorporation of Cr and Li codopants is also supported by the variation of the luminescence behavior with respect to the reference samples, as explained in detail below.

The temperature window for achieving the growth of elongated microstructures of tin oxide depends on the selected precursor. The growth temperature ranges between 1300 and 1400 ºC when using tin oxide as precursor. In order to lower the growth temperature to around 600 ºC other precursors could be used as metallic tin,[30-31] which also changes the morphology and reduces the size of the obtained structures giving raise mainly to the growth of nanowires. Alternatively, microstructures could be obtained at intermediate temperatures around 900ºC by adding to metallic tin powders a high amount of metallic copper. In this case, copper is introduced as a dopant into the tin oxide rutile structure and the final morphology are microrods and belts, as shown in Figure 4(a) and 4(b) for a Cu:Sn ratio of 2:1. The highest

copper content is obtained in the belts and quantified around 3 cationic % by EDS (see EDS Sn and Cu mappings in Figure 4(c-d)). The Cu doped SnO_2 microbelts have been characterized by XRD, as it is shown in Figure 4(e), which can be indexed with the tin oxide rutile structure, as it can be in the shown in the spectrum. Ternary compounds, intermediate phases or metallic Cu or Sn from the precursors have been discarded, as an indicative of an adequate diffusion of Cu atoms into the SnO_2 lattice during the thermal treatment, in good agreement with the homogeneous distribution of Sn and Cu along the grown microbelts observed in the EDS mappings.

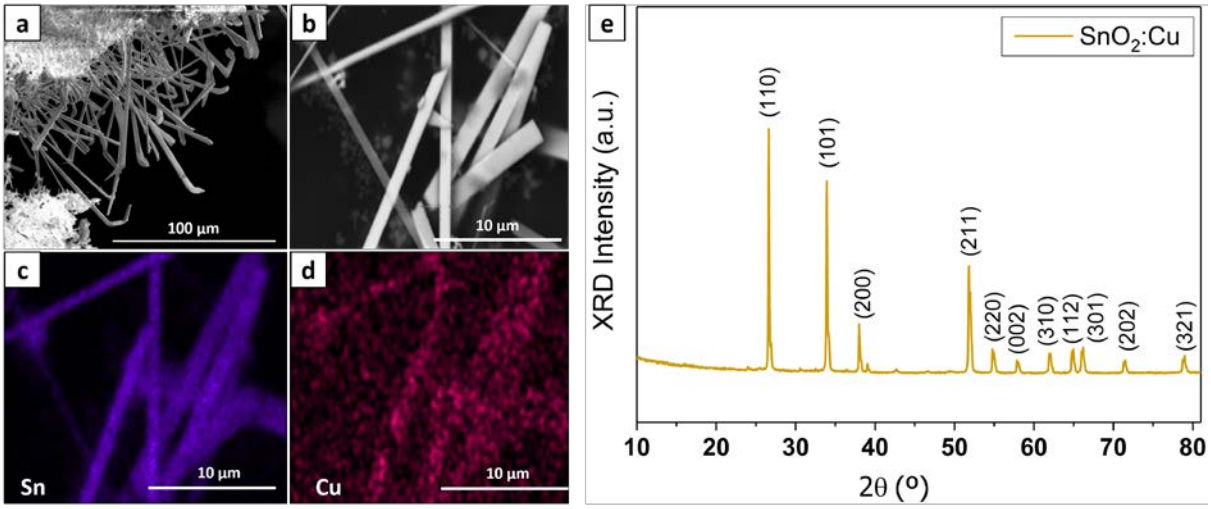

Figure 4. SEM images of the microstructures present in the Cu doped sample: (a) microrods and (b) belts, (c)-(d) EDS mapping of elemental Sn and Cu corresponding to the belts of (b), respectively and (e) XRD pattern of Cu doped SnO_2 samples.

In order to achieve a better understanding of our system, the CL spectra at low temperature of the Cu doped and Li-Cr codoped SnO_2 microstructures are shown for comparison with the spectra of the reference materials in Figure 5(a).

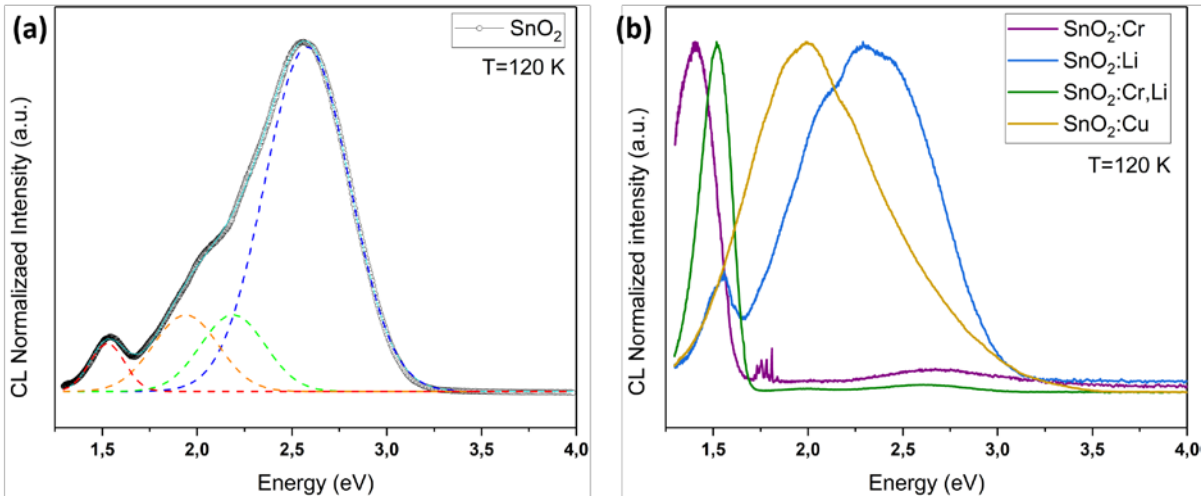

Figure 5. (a) CL spectra acquired on the undoped microtubes, (b) Cr doped, Li doped Cu doped and codoped SnO_2:Cr,Li samples.

As observed in Figure 5(a), the CL spectrum of undoped tubes SnO_2 consists of a wide visible emission with four different contributions centered at 1.5, 1.98, 2.25 and 2.58 eV, respectively. The first emission at 1.5 eV presents a reduced intensity and is scarcely reported for undoped tin oxide material. Some authors[32] have attributed this NIR band to a high surface density of defects states, which is in agreement with the high surface/volume ratio that exhibit the microstructures describe in this work. The orange (1.98 eV) and the green emission (2.25 eV) are associated with oxygen vacancies[21] and complex defects involving oxygen vacancies,[21] while the blue emission (2.58 eV), is related to surface states.[21, 33]

The incorporation of Li modifies the CL response by promoting the emission around 1.5 eV, as explained by F. del Prado *et al.*[28] On the other hand, no sharp lines were observed in the SnO_2:Li spectrum at about 1.70 eV (729.32 nm) corresponding to ^2S-$^2P_0$ intraionic transitions due to Li^+ in other TCO's such as Ga_2O_3 or TiO_2 as reported by some authors.[34-35] An allowed transition, $^2P_0$-^2S attributed to Li^+ cations,[36] centered at 1.52 eV (815.8 nm) has also been reported. However, in our case the broad NIR emission at 1.52 eV is detected not only in the Li doped microstructures but also in the undoped ones, as shown in Figure 5(a). Therefore, an origin related to Li intraionic emissions can be disregarded in this case. A

similar radiative recombination observed in Cu, Co and Fe doped SnO_2 films have been attributed by Korotcenkov *et al.*[37] to Sn interstitials. Analogously, in our samples a band at around 1.65 eV is induced by Cu doping, although with reduced relative intensity, as compared to the Li doping samples. The state of charge of copper incorporated in the tin oxide rutile structure is unknown. Preferential incorporation of copper as Cu^{2+} could be presumed, as this ion is more stable than the Cu^{+} ion, although further direct measurements are needed to properly asses this point as well as the probability to find Cu ions in both states of charge. For both samples, Li and Cu doped ones, the intrinsic visible bands of tin oxide are the main contribution to the luminescence of the structures, although the relative intensity of the different visible bands is not the same after the introduction of Li or Cu. Doping SnO_2 with Cr introduces two main differences in the SnO_2 CL emission spectra. The first one is the emission centered at 1.79 eV associated with intraionic transitions of Cr^{3+} in octahedral positions.[38] The second one is the new emission located around 1.4 eV associated with intrinsic defects present in SnO_2 and promoted by doping.[29] In the SnO_2:Cr doped samples, a small contribution from the blue SnO_2 emission still remains.

The CL spectrum of the codoped sample SnO_2:Cr,Li consists of a narrow and intense emission in the near-IR, centered at about 1.5 eV (≈825 nm), and a weak emission centered at around 2.7 eV (≈477 nm). The luminescence has been successfully shifted to the near infrared for the codoped samples, which could turn in new applications of tin oxide as for example in bio-imaging. The NIR luminescence of the Cr-Li codoped SnO_2 samples have been analyzed in more detail. The CL spectra acquired in the sample at different temperatures ranging from 120-300 K can be observed in Figure 6, where it can be appreciated a clear increase in the total CL signal as the temperature decreases.

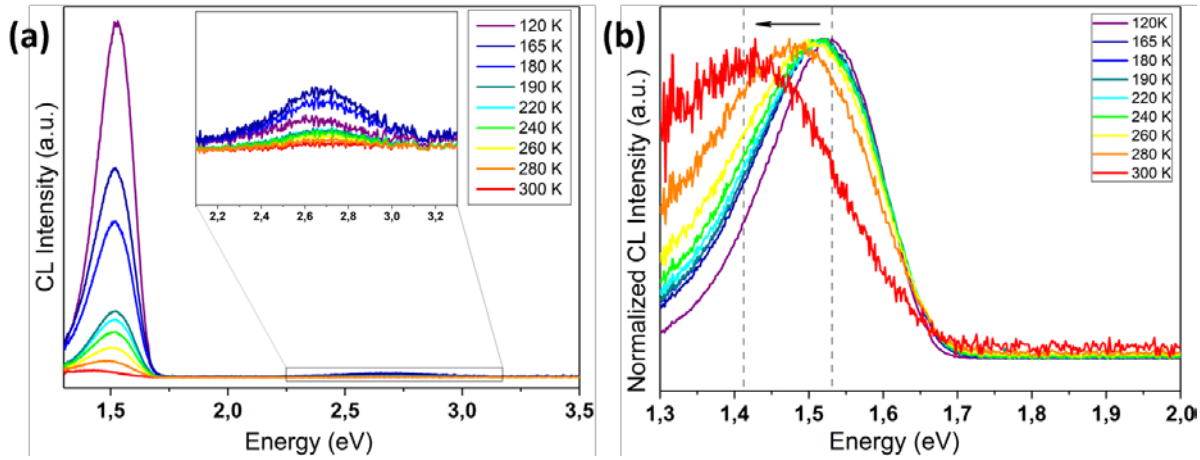

Figure 6. (a) CL spectrum acquired on a microtube of a codoped SnO_2:Cr,Li sample at different temperatures, with an inset showing and enlargement of the visible emission. (b) Normalized CL spectra of the NIR region.

At the inset in Figure 8(a) an enlargement of CL visible emission is shown. The main band centered at around 2.7 eV is totally quenched as the temperature increases up to 300 K. According to the normalized CL spectra shown in Figure 8(b), the maximum in the emission of the SnO_2:Cr,Li samples appears to be centered at 1.55 eV at low temperatures and a slight shift towards 1.42 eV is observed as temperature increases up to 300 K. This result could indicate that this emission is a complex band composed by the contributions at 1.4 and 1.6 eV from Cr and Li ion respectively which evolve differently with temperature. However, the observed behavior with temperature is also characteristic of radiative transitions involving charge transfer,[39] and other complex defects involving Li and Cr ions cannot be disregarded. Furthermore, Li codoping is a common strategy to enhance efficiency in phosphors[40] and several mechanisms could contribute to this effect, among others charge compensation as Li^+ can compensate the cationic vacancies produced by the incorporation of trivalent or divalent ions to phosphor materials and eventually promote more ions incorporating into the host lattice.

In summary, the observed luminescence of doped samples should be tentatively related to the effects of the incorporation of dopants into the rutile lattice of tin oxide, which could induce

the generation of a complex defect to compensate the charge imbalance due to the substitution of tin by Li, Cu, or Cr, respectively. The final peak position seems to be related to the specific dopant element, as for Cr doped samples the NIR emission is centered at around 1.4 eV, for Li and Cu doping it moves towards higher energies around 1.6 eV, meanwhile for Li-Cr codoped samples its position is around 1.5 eV.

3. Conclusion

Doping tin oxide during a vapor-solid growth using Li, Cu and Cr containing precursors in the initial mixture enables the achievement of near infrared luminescence from tin oxide low dimensional structures. The best results are achieved by codoping tin oxide with Li and Cr, obtaining single crystalline microtubes by a vapor-solid growth at 1400 ºC. The tubes exhibit an intense luminescence at around 1.5 eV with simultaneous quenching of the visible emission band of tin oxide. Unravelling the origin of this luminescence band needs further research, although our results suggest its relation to intrinsic tin oxide defects generated to compensate charge imbalance due to the incorporation of the doping elements into the tin oxide lattice. This band seems to be composed by several contributions depending on the charge state of the doping element. Although copper doping does not promote the quenching of the visible band, it also allows a NIR emission around 1.6 eV, meanwhile the morphology variability increases, obtaining rods and belts at lower treatment temperatures.

4. Experimental Section

SnO_2 nano and microstructures were fabricated following a vapor-solid mechanism by thermal treatments of SnO_2 powders under controlled Ar flow. Doping with Cu or codoping with Li and Cr was achieved during the growth by selecting a convenient mixture of the following commercial powders as starting materials: SnO_2 (Sigma-Aldrich, 99.9%), metallic Sn (Sigma-Aldrich, 99%), metallic Cu (Sigma-Aldrich, 99 %), Li_2CO_3 (Labkem, 99.0%) and Cr_2O_3 (Sigma-Aldrich, 99.9%). After several experiments, a 5 % weight concentration of Li

and Cr in the initial mixture with SnO_2 powders was chosen for the growth of Li-Cr codoped samples, meanwhile for Cu doping the starting mixture contained a weight ratio of metallic Cu to Sn of 2:1. The obtained samples are named hereinafter, SnO_2:Cu, and SnO_2:Cr,Li for doped and codoped samples, respectively. Undoped samples and samples doped with only Cr or Li are also used in this work as reference materials, and will be named as SnO_2, SnO_2:Cr, and SnO_2:Li, respectively. The fabrication and characterization of the reference materials have been reported elsewhere.[22, 28-29]

In order to obtain the precursor material, a milling process was carried out in order to homogenize the corresponding powder mixture, by using a mechanical agate ball mill (in a Restch S100) during 5 hours at 150 rpm. The homogenized powders were pressed into a pellet (7 mm diameter, ~3 mm high) using a MEGA KP-30th mechanical press. Afterwards, the pellets were introduced in a furnace under an argon flow. The thermal treatments were carried out during 10 hours in a MUFLA RHF Carbolite 1500 with an Ar flow of 1.5 L/min at temperatures between 900-1400 °C. Specifically, for the undoped SnO_2, SnO_2:Cr and SnO_2:Cr,Li samples the optimized temperature was 1400 °C, whereas for the sample SnO_2:Li the temperature employed was 1350°C and for Cu doping the temperature was 900 ºC.

The obtained microstructures were studied by X-Ray Diffraction (XRD) using a Panalytical X'Pert Pro Alpha1 diffractometer with the working radiation of Cu (K_α) (λ = 1.5418 Å). The morphology of the as grown samples was studied by scanning electron microscopy (SEM) in a Leica 440 Stereoscan and a FEI-Inspect S at accelerating voltages of between 15-20 kV. The luminescence of the samples was also studied at variable temperature by cathodoluminescence (CL) in a Hitachi S-2500. Compositional analysis was performed by energy-dispersive x-ray spectroscopy in a SEM, using an XFlash 4010 detector.

Acknowledgements

The work was supported by MINECO/FEDER projects: MAT 2016-81720-REDC and MAT 2015-65274-R. The authors are grateful to Prof. Javier Piqueras (Universidad Complutense de Madrid) for being an inspiring reference in their research careers.

Received: ((will be filled in by the editorial staff))
Revised: ((will be filled in by the editorial staff))
Published online: ((will be filled in by the editorial staff))

References

[1] Zhang, Y.; Kolmakov, A.; Chretien, S.; Metiu, H.; Moskovits, M., Control of catalytic reactions at the surface of a metal oxide nanowire by manipulating electron density inside it. *Nano Letters* **2004,** *4* (3), 403-407.

[2] Li, Z. D.; Zhou, Y.; Yu, T.; Liu, J. G.; Zou, Z. G., Unique Zn-doped SnO_2 nano-echinus with excellent electron transport and light harvesting properties as photoanode materials for high performance dye-sensitized solar cell. *Crystengcomm* **2012,** *14* (20), 6462-6468.

[3] Wang, W. W.; Zhu, Y. J.; Yang, L. X., ZnO-SnO2 hollow spheres and hierarchical nanosheets: Hydrothermal preparation, formation mechanism, and photocatalytic properties. *Advanced Functional Materials* **2007,** *17* (1), 59-64.

[4] Kim, C.; Noh, M.; Choi, M.; Cho, J.; Park, B., Critical size of a nano SnO_2 electrode for Li-secondary battery. *Chemistry of Materials* **2005,** *17* (12), 3297-3301.

[5] Archer, P. I.; Radovanovic, P. V.; Heald, S. M.; Gamelin, D. R., Low-temperature activation and deactivation of high-Curie-temperature ferromagnetism in a new diluted magnetic semiconductor: Ni^{2+}-Doped SnO_2. *J Am Chem Soc* **2005,** *127* (41), 14479-87.

[6] Zhang, L.; Ge, S.; Zuo, Y.; Wang, J.; Qi, J., Ferromagnetic properties in undoped and Cr-doped SnO_2 nanowires. *Scripta Materialia* **2010,** *63* (10), 953-956.

[7] Garcia-Tecedor, M.; Maestre, D.; Cremades, A.; Piqueras, J., Influence of Cr Doping on the Morphology and Luminescence of SnO_2 Nanostructures. *Journal of Physical Chemistry C* **2016,** *120* (38), 22028-22034.

[8] Wang, C. T.; Chen, M. T.; Lai, D. L., Vanadium‐Tin Oxide Nanoparticles with Gas‐Sensing and Catalytic Activity. *Journal of the American Ceramic Society* **2011,** *94* (12), 4471-4477.

[9] Peche-Herrero, M. A.; Maestre, D.; Ramirez-Castellanos, J.; Cremades, A.; Piqueras, J.; Gonzalez-Calbet, J. M., The controlled transition-metal doping of SnO_2 nanoparticles with tunable luminescence. *Crystengcomm* **2014,** *16* (14), 2969-2976.

[10] Herrera, M.; Maestre, D.; Cremades, A.; Piqueras, J., Growth and Characterization of Mn Doped SnO_2 Nanowires, Nanobelts, and Microplates. *The Journal of Physical Chemistry C* **2013,** *117* (17), 8997-9003.

[11] Chi, J.; Ge, H.; Wang, J.; Zuo, Y.; Zhang, L., Synthesis and electrical and magnetic properties of Mn-doped SnO2 nanowires. *Journal of Applied Physics* **2011,** *110* (8), 083907.

[12] Wu, J.; Coffer, J. L., Strongly emissive erbium-doped tin oxide nanofibers derived from sol gel/electrospinning methods. *The Journal of Physical Chemistry C* **2007,** *111* (44), 16088-16091.

[13] del-Castillo, J.; Rodríguez, V.; Yanes, A.; Méndez-Ramos, J., Energy transfer from the host to Er^{3+} dopants in semiconductor SnO_2 nanocrystals segregated in sol–gel silica glasses. *Journal of Nanoparticle Research* **2008,** *10* (3), 499-506.

[14] Santilli, C. V.; Pulcinelli, S. H.; Brito, G.; Briois, V., Sintering and crystallite growth of nanocrystalline copper doped tin oxide. *The Journal of Physical Chemistry B* **1999,** *103* (14), 2660-2667.

[15] Niranjan, R.; Patil, K.; Sainkar, S.; Mulla, I., High H_2S-sensitive copper-doped tin oxide thin film. *Materials chemistry and physics* **2003,** *80* (1), 250-256.

[16] Liu, S.-J.; Liu, C.; Juang, J.; Fang, H., Room-temperature ferromagnetism in Zn and Mn codoped SnO_2 films. *Journal of Applied Physics* **2009,** *105* (1), 013928.

[17] Nomura, K.; Okabayashi, J.; Okamura, K.; Yamada, Y., Magnetic properties of Fe and Co codoped SnO_2 prepared by sol-gel method. *Journal of Applied Physics* **2011,** *110* (8), 083901.

[18] Eustache, E.; Tilmant, P.; Morgenroth, L.; Roussel, P.; Patriarche, G.; Troadec, D.; Rolland, N.; Brousse, T.; Lethien, C., Silicon‐Microtube Scaffold Decorated with Anatase TiO_2 as a Negative Electrode for a 3D Litium‐Ion Microbattery. *Advanced Energy Materials* **2014,** *4* (8).

[19] Bae, C.; Yoo, H.; Kim, S.; Lee, K.; Kim, J.; Sung, M. M.; Shin, H., Template-directed synthesis of oxide nanotubes: fabrication, characterization, and applications. *Chemistry of Materials* **2008,** *20* (3), 756-767.

[20] Vasquez, G. C.; Peche-Herrero, M. A.; Maestre, D.; Cremades, A.; Ramirez-Castellanos, J.; Gonzalez-Calbet, J. M.; Piqueras, J., Cr doped titania microtubes and microrods synthesized by a vapor-solid method. *Crystengcomm* **2013,** *15* (27), 5490-5495.

[21] Maestre, D.; Cremades, A.; Piqueras, J., Growth and luminescence properties of micro- and nanotubes in sintered tin oxide. *Journal of Applied Physics* **2005,** *97* (4), 044316.

[22] Maestre, D.; Cremades, A.; Piqueras, J.; Gregoratti, L., Thermal growth and structural and optical characterization of indium tin oxide nanopyramids, nanoislands, and tubes. *Journal of Applied Physics* **2008,** *103* (9), 093531.

[23] Garcia-Tecedor, M.; del Prado, F.; Bueno, C.; Vasquez, G. C.; Bartolome, J.; Maestre, D.; Diaz, T.; Cremades, A.; Piqueras, J., Tubular micro- and nanostructures of TCO materials grown by a vapor-solid method. *Aims Materials Science* **2016,** *3* (2), 434-447.

[24] Maestre, D.; Hernández, E.; Cremades, A.; Amati, M.; Piqueras, J., Synthesis and Characterization of Small Dimensional Structures of Er-Doped SnO_2 and Erbium–Tin–Oxide. *Crystal Growth & Design* **2012,** *12* (5), 2478-2484.

[25] García-Tecedor, M.; Maestre, D.; Cremades, A.; Piqueras, J., Tailoring optical resonant cavity modes in SnO_2 microstructures through doping and shape engineering. *Journal of Physics D: Applied Physics* **2017,** *50* (41), 415104.

[26] Maestre, D.; Cremades, A.; Piqueras, J., Cathodoluminescence of defects in sintered tin oxide. *Journal of Applied Physics* **2004,** *95* (6), 3027-3030.

[27] Smith, E. J.; Schulze, S.; Kiravittaya, S.; Mei, Y.; Sanchez, S.; Schmidt, O. G., Lab-in-a-tube: detection of individual mouse cells for analysis in flexible split-wall microtube resonator sensors. *Nano letters* **2010,** *11* (10), 4037-4042.

[28] del Prado, F.; Cremades, A.; Ramírez-Castellanos, J.; Maestre, D.; González-Calbet, J. M.; Piqueras, J., Effect of lithium doping and precursors on the microstructural, surface

electronic and luminescence properties of single crystalline microtubular tin oxide structures. *CrystEngComm* **2017,** *19* (30), 4321-4329.

[29] Garcia-Tecedor, M.; Maestre, D.; Cremades, A.; Piqueras, J., Growth and characterization of Cr doped SnO_2 microtubes with resonant cavity modes. *Journal of Materials Chemistry C* **2016,** *4* (24), 5709-5716.

[30] Duan, J.; Yang, S.; Liu, H.; Gong, J.; Huang, H.; Zhao, X.; Zhang, R.; Du, Y., Single crystal SnO_2 zigzag nanobelts. *Journal of the American Chemical Society* **2005,** *127* (17), 6180-6181.

[31] Junhong, D.; Jiangfeng, G.; Hongbo, H.; Xiaoning, Z.; Guangxu, C.; Zhong-Zhen, Y.; Shaoguang, Y., Multiform structures of SnO_2 nanobelts. *Nanotechnology* **2007,** *18* (5), 055607.

[32] Wang, D. N.; Yang, J. L.; Li, X. F.; Wang, J. J.; Li, R. Y.; Cai, M.; Sham, T. K.; Sun, X. L., Observation of Surface/Defect States of SnO_2 Nanowires on Different Substrates from X-ray Excited Optical Luminescence. *Crystal Growth & Design* **2012,** *12* (1), 397-402.

[33] Fillard, J. P.; Demurcia, M., Low-Temperature Photoluminescence in SnO_2 High-Resistivity Monocrystals. *Physica Status Solidi a-Applied Research* **1975,** *30* (1), 279-287.

[34] Lopez, I.; Alonso-Orts, M.; Nogales, E.; Mendez, B.; Piqueras, J., Influence of Li doping on the morphology and luminescence of Ga_2O_3 microrods grown by a vapor-solid method. *Semiconductor Science and Technology* **2016,** *31* (11), 115003.

[35] Kallel, W.; Bouattour, S.; Ferreira, L. V.; do Rego, A. B., Synthesis, XPS and luminescence (investigations) of Li^+ and/or Y^{3+} doped nanosized titanium oxide. *Materials Chemistry and Physics* **2009,** *114* (1), 304-308.

[36] Wiese, W. L.; Fuhr, J. R., Accurate Atomic Transition Probabilities for Hydrogen, Helium, and Lithium. *Journal of Physical and Chemical Reference Data* **2009,** *38* (3), 565-720.

[37] Korotcenkov, G.; Cho, B. K.; Nazarov, M.; Noh, D. Y.; Kolesnikova, E. V., Cathodoluminescence studies of un-doped and (Cu, Fe, and Co)-doped tin dioxide films deposited by spray pyrolysis. *Current Applied Physics* **2010,** *10* (4), 1123-1131.

[38] Nogales Díaz, E.; García, J. A.; Méndez Martín, B.; Piqueras de Noriega, J., Red luminescence of Cr in ß-Ga_2O_3 nanowires. *Journal of applied physics* **2007,** *101* (3).

[39] Ye, S.; Song, E. H.; Zhang, Q. Y., Transition Metal ‐ Involved Photon Upconversion. *Advanced Science* **2016,** *3* (12).

[40] Chen, J.; Li, C.; Hui, Z.; Liu, Y., Mechanisms of Li^+ ions in the emission enhancement of $KMg_4(PO_4)_3$: Eu^{2+} for white light emitting diodes. *Inorganic chemistry* **2017,** *56* (3), 1144-1151.

Table of Contents (ToC)

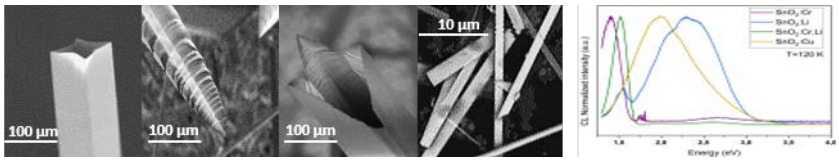

Doping tin oxide with Li, Cu and Cr enables the achievement of near infrared luminescence from tin oxide microstructures. In the present work, different doped low dimensional structures have been obtained by a vapor-solid method. Luminescence around 1.5 eV is obtained for all the samples with morphologies varying from microtubes to belts depending on the specific dopant and the Sn-based precursor.